DOI: https://doi.org/10.31351/vol34iss2pp122-143

Synthesis, Characterization and Anticancer Activity of some Metal Complexes of New Ligand Derived from 4-Methylbenzohydrazide with Computational Studies

Enass J. Waheed[*,1]

[1]Department of Chemistry, College of Education for Pure Sciences, Ibn -Al-Haitham, University of Baghdad, Baghdad, Iraq
[*]**Corresponding Author**
Received 22/10/2023, Accepted 28/2/2024, Published 25/6/2025

Abstract

This research aims to prepare a set of complexes with the general formula [M(HMB)n] , where M=VO (II) , Cr(III) ,and Cu(II), while n=2,3,2 respectively, resulting from the reaction of a new ligand [N'-(2-hydroxy-3-methoxybenzyl)-4-methylbenzohydrazide] (HMB) derived from the reaction of the two substances (4-methylbenzohydrazide and 2-hydroxy-3-methoxy benzaldehyde) with metal ions. The prepared compounds were identified by several spectroscopic methods, such as infrared, nuclear magnetic resonance, and electronic spectra. From the results of the measurements, it was suggested that the prepared complexes have different geometries, such as square planar (Cu), pyramidal (VO), and octahedral (Cr). DFT simulations backed up the experimental evidence. The geometries of ligand (HMB) and its complexes were thoroughly optimized using Gaussian 09w in DFT calculations, and numerous molecular characteristics were determined as well. The results showed that the metal complexes investigated are more stable than the free ligand (HMB). Molecular docking was used on E. coli and S. aureus proteins to estimate the probable binding energy of inhibitors. The activity of the compounds to inhibit different types of bacteria *E. coli* (negative) and *S. aureus* (positive) was investigated. where investigations revealed that the Cu-complex exhibited a stronger capacity to inhibit both types of bacteria than the ligand (HMB). The ligand and its copper complex were investigated for anticancer activity against HepG2 cells and normal cell WRL-68.

Keywords: anticancer Activity, density functional theory, metal complexes, 4-methylbenzohydrazide, molecular docking.

Introduction

Benzohydrazide derivatives are important compounds in organic synthesis and have various biological activities, such as anti-leishmanial, anti-inflammatory, anti-cancer, anti-mycobacterial, and their applications in medicinal and analytical chemistry [1, 2]. 4-Methoxybenzhydrazide is used as a pharmaceutical intermediate and it is also involved in a variety of organic synthesis ,while 2-hydroxy-3-methoxy benzaldehyde is a naturally occurring aldehyde used as a flavoring product and in treating abdominal pain. One of the most important applications of metal complexes is that they are antibacterial and anti-cancer. Among the metal complexes, vanadium, chromium, and copper complexes have been shown to exhibit significant biological activities [3-5].

Copper compounds have proven their potential to promote biological activity over time. This is due to the fact that copper compounds have a wide variety of pharmacological activities, including anti-inflammatory, anti-cancer, and antibacterial properties [6]. Copper's ability to coordinate with organic or inorganic biomolecules, establishing novel complexes with improved oral bioavailability and pharmacological profiles, is just one of many features that give copper the advantage of being less toxic than the majority of the 4d and 5d transition metals[7]. Copper and its complexes are significant *in vitro* investigations, in vivo research, and clinical studies, and their interest arises from their potential therapeutic uses in a range of disorders. One of the most pressing concerns in this field is developing novel chemicals that are effective against cancer cells in particular while minimizing negative effects. Copper's various coordination numbers and oxidation states, which allow it to interact with a wide range of ligand bases, provide a broad foundation for the creation of anti-cancer medicines [8].

In this research, we have synthesized the VO (II) , Cr(III) and Cu(II) complexes of a new ligand [N'-(2-hydroxy-3-methoxybenzyl)-4-methylbenzohydrazide] (HMB) derived from the reaction of the two substances 4-methylbenzohydrazide and 2-hydroxy-3-methoxy benzaldehyde and characterized by several

spectroscopic methods. Molecular docking, DFT properties, and biological activity of the prepared compounds were also studied (antibacterial, anticancer).

Materials and Methods

From commercial places of certified international companies, the chemicals and solvents found in the work were purchased as they were used without purification. Using a UV-visible spectrophotometer (Shimadzu UV-1800) at a concentration of 10^{-3}M in solvent $(CH_3)_2SO$ at room temperature and 1.0 cm for a quartz cell length, the electronic spectra of prepared compounds were diagnosed. Using spectrophotometer (Biotic. 600 FTIR) of the KBr in the range (4000 - 400)cm^{-1} was determined frequencies of the active groups of the prepared compounds were determined. Using Bruker Avance 400 Ultra Shield NMR, which originated in Germany, ^{1}H and^{13}C-NMR spectra were recorded for the bonds in DMSO-d6. All isolates were tested in the laboratory for their biological control ability were provided from National Center for Educational Laboratories Elemental microanalysis were carried out on a perkin elmer 2400 LS Series CHN Analyzer, at Kharazmi University, Iran.

Synthesis of the new ligand [N'-(2-hydroxy-3-methoxybenzyl)-4-methylbenzohydrazide] (HMB)

Step1: (E)-N'-(2-hydroxy-3-methoxybenzylidene)-4-methylbenzohydrazide

This compound was synthesized using the procedure described by Rao et al.[9]. To a stirred solution of 2-hydroxy-3-methoxybenzaldehyde (0.25 g, 1.64 mmol) in 10 mL of absolute ethanol with (3) drops of acetic acid, a solution of 4-methylbenzohydrazide (0.25 g, 1.64 mmol) was added in 10 ml of absolute ethanol in small portions. The component was to leave within 3 h (reflux). The precipitate was collected, washed with cold ethanol, dried after being cooled to room temperature, and given a yellow precipitate after recrystallization with ethanol.

Step2: Synthesis of N'-(2-hydroxy-3-methoxybenzyl)-4-methylbenzohydrazide

This compound was synthesized according to procedure [10]. Small portions of sodium boro hydride (0.062 g, 1.64 mmol) were added to a stirring solution of compound (**Step1**) in 10 ml of tetra hydro furane: methanol (1:1). After completion, add 15 ml of crushed ice and stirred the mixture vigorously for half an hour. The precipitate was collected by filtration and recrystallized after drying in aqueous methanol to give off-white crystals. m.p. 225-227 °C (yield 76%) ,Scheme 1.

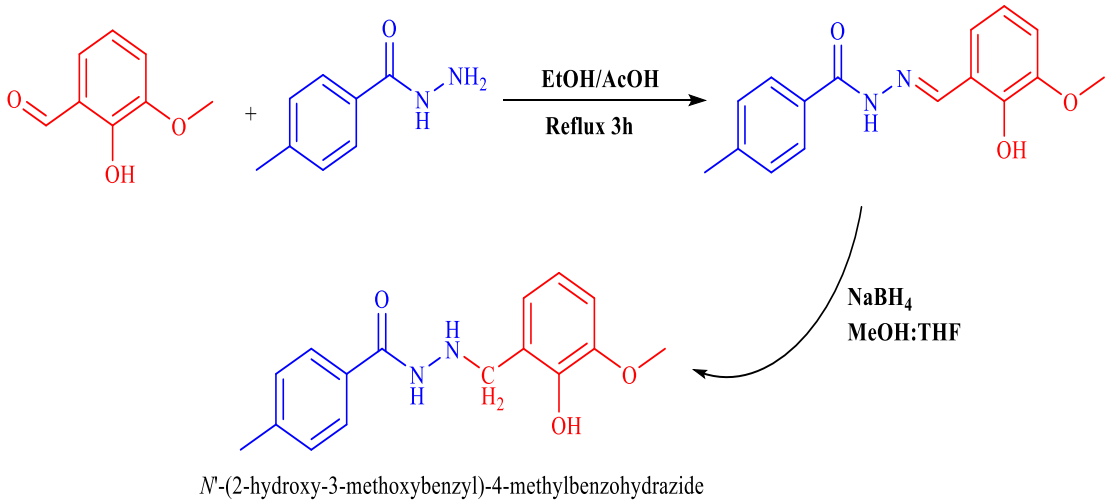

Scheme 1. Synthesis of the ligand (HMB) in two steps

General procedure of copper, vanadium oxide, and chrome

The complex was synthesized according to procedure[11, 12]. The molar ratio (1:2) of metal:(HMB). The metal chloride ($CuCl_2.2H_2O$) (0.3gm, 1.75mmol) in (10 ml) ethanol was added to the ethanolic base solution (10ml) of ligand (HMB) (1gm, 3.49 mmol). At 70°C, leave the mixture with continuous stirring and reflux (3-4) hours. The precipitate was filtered, washed by mix (evaporate water and diethyl ether), and recrystallized by absolute ethanol; the color is bluish green. The yield % of $[Cu(HMB)_2]$ was 85%, in Figure 1 structure of complexes.

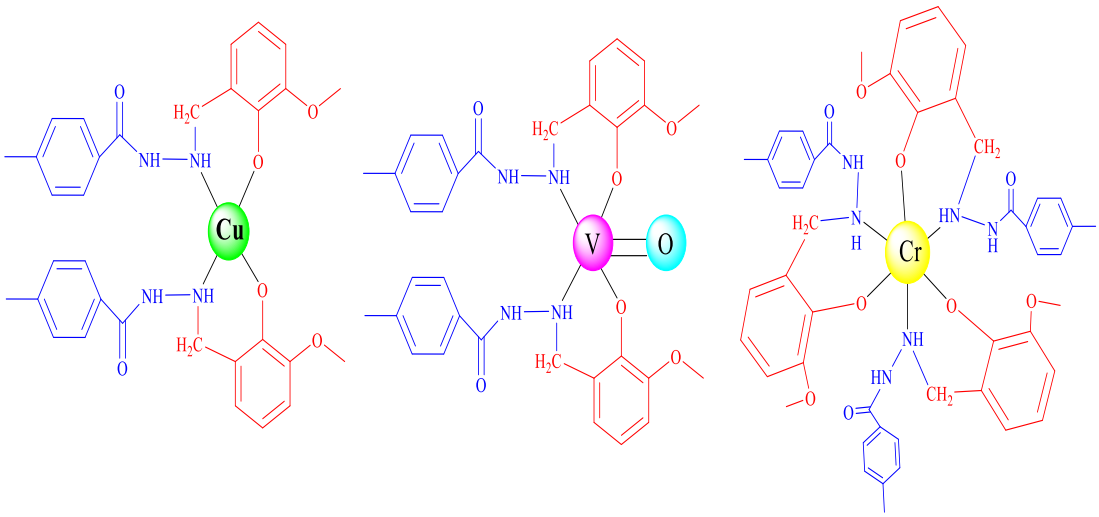

Bis[N'-(2-hydroxy-3-methoxybenzyl)-4-methylbenzohydrazide]Copper(II) (1)

Bis[N'-(2-hydroxy-3-methoxybenzyl)-4-methylbenzohydrazide]Vanadyl(II) (2)

Tris[N'-(2-hydroxy-3-methoxybenzyl)-4-methylbenzohydrazide]Chromium(III) (3)

Figure 1. Structure of complexes (1, 2 and 3)

Docking method

The proteins chosen for this work were serine protease SplB (2vid) for *Staphylococcus aureus* bacteria and *Rhomboid-protease*-GLPG (3zmj) for *Escherichia coli* bacteria, both downloaded from the NCBI database website https://www.ncbi.nlm.nih.gov. Downloaded proteins were prepared before docking (removing water, adding charge, fixing the terminals, etc.) with the Autodock Vina software included in the MGL 1.5.7 package. The docking process was performed without specifying the active site location (blind docking method) using the CB-dock online tool.

Biological Study

A- Culture Media

The medium was prepared via manufacturers, and then sterilized for 15 minutes at 121°C , then left to cool to 37°C for use to get a single pure colony.

1- MacConkey agar (oxoid-UK)

This media was prepared by suspend 52g in 1 liter distill water and stirring until dissolved until dissolve. Sterilized by autoclave for 15 minutes at 121°C.

2- SS agar (oxoid-UK)

To prepare this media 63g of ready media was dissolved in1000 0f D.W and gently heated until it completely dissolved. and autoclaved at 121°C for 20 minutes. Cooled to about 37°C, an aliquot of 10ml was dispensed into sterile Petri dishes.

3- Mannitol salt agar (oxoid-UK)

Commonly used selective and differential growth mediums in microbiology. 111 g of MS media dissolved in 1000 ml of distilled water were heated until completely dissolved. At 121°C for 15 minutes, it was sterilized by an autoclave.

4- Muller Hinton agar (oxoid-UK)

38g of media was added to 1 liter of distilled water. Sterilize by autoclave at 121°C for 15 minutes.

B- In vitro screening for Antibacterial:

Using double inoculation techniques, all isolates were tested in the laboratory for their biological control ability was providing from National Center for Educational Laboratories. Using Mueller-Hinton agar to determine compatibility and antagonistic reactions, double-culture assay was performed. The test was done by drawing a single colony from a 24-hour culture on Mueller-Hinton agar. A sterile cork borer was used to dig wells, and 50 µl of 10^{-3} v\con dilution in (Distilled water) were poured into each well. The plates were subsequently incubated for 18 hours at 37°C, and the percentage of inhibition and redial growth was calculated.

Anticancer Study

By studying their ability to inhibit cell proliferation (HepG2), the anti-proliferative activity of the prepared compounds was tested. The effect of cytotoxic compounds was examined using the MTT test in 96 plates, after which the cells were treated with the prepared compounds after 24 hours or when a confluent monolayer was created. After 24 hours of treatment, cell viability was determined by removing µl/well MTT medium solutions and incubating them for 4 hours. The MTT solution was removed at 37°C, and then the crystals in the wells were dissolved by adding 200 µL of DMSO and incubating for 15 minutes at 37°C with shaking. Using a microplate reader, absorbance was measured at 620 nm.

Results and Discussion

The prepared compounds are characterized by being stable at laboratory temperature and soluble in some organic solvents, including DMSO, as it was considered a suitable solvent for conducting the required measurements, including the molar conductivity of the three prepared complexes, which fall within the range (15-23) $\Omega^{-1}cm^2mol^{-1}$, and this indicates their non-electrolytic nature.

For the purpose of discussing reaction, Sodium borohydride ($NaBH_4$) is a convenient source of hydride ion (H^-) for the reduction of Schiff base to produce compound (HMB). Nevertheless, an alcohol, often methanol or ethanol and THF [1:1] , is generally the solvent of choice for sodium borohydride reductions of schiff base, When $NaBH_4$ is used in a reaction, it donates a hydride ion to the double bond HC=N, resulting in the reduction of the bond to a single bond CH_2-NH. This proceeds via a two-step mechanism consisting of nucleophilic addition, followed by protonation. Where the FT-IR of compound (HMB) displayed new band of NH distinctly. Table 1. show the different physical properties and CHN data, chemical formula, melting temperatures, color, and yields of the prepared compounds.

Table 1. The BDS properties and its complexes

Com.	M . wt g /mol	m.p°C	Color	Elemental Microanalysis (%)			
				M	C	H	N
$C_{16}H_{18}N_2O_3$ (HMB)	286.33	225-227	Off white	-----	67.90	6.32	9.79
$C_{32}H_{34}VN_4O_7$	637.59	181-183	Desert	7.70	60.01	5.10	8.83
$C_{48}H_{51}CrN_6O_9$	907.97	199-201	Brown	5.55	63.83	5.90	9.25
$C_{32}H_{34}CuN_4O_6$	634.18	176-178	Green	10.40	60.52	5.41	8.84

Results and Discussion

^{1}H & ^{13}C-NMR Spectra of ligand (HMB)

The results ^{1}H & ^{13}C-NMR spectra of (HMB) are shown below [13-15], Figure 2(a and b).

^{1}H NMR: 2.43 S, CH_3, 3H**;** 3.81 S, CH_2N, 2H**;** 3.85 S, OCH_3, 3H**;** 5.55 bs, OH, 1H**;** 6.75 t, H4, 1H**;** 7.08 d, H3, 1H**;** 7.17 d, H5, 1H**;** 7.29 d, H10, 2H**;** 7.39 d, H11, 2H**;** 11.08 bs, NH**;** 12.06 bs, NH.

^{13}C NMR: 21.55 1C, C13, CH_3**;** 51.28 1C, C7, CH_2N**;** 58.31 1C, C14, OCH_3**;** 111.65 1C, C3**;** 121.32 1C, C5**;** 122.07 1C, C4**;** 127.62 2C, C10**;** 129.45 1C, C9**;** 129.64 2C, C11**;** 130.41 1C, C6**;** 141.59 1C, C12**;** 142.52 1C, C1**;** 147.90 1C, C2**;** 165.76 1C, C8, C=O.

FT-IR Spectra of prepared compounds

The position of the important bands of prepared compounds is shown in Table 2. The ligand (HMB) exhibited characteristic υ(N-H) stretching frequencies at (3315), which shift to higher frequencies in range (3483-3419), upon complexation .This indicates the participation of hydrazide nitrogen in bonding . The FTIR spectrum of the free ligand shows bands at (3263) cm^{-1} due to the phenolic υ(OH) group for (HMB). The reason for the shift to higher or lower frequencies is attributed to the presence of coordination between the ligand and the metal ion. Among the important factors that affect the frequency shift are the donor atoms and the nature of the metal ion. The absence of these bands in the spectra of all complexes and adducts indicates the coordination of phenolic (O) to the metal after deprotonation. This is further confirmed by the shifting of υ (CO) phenolic bands (1246,1190) cm^{-1} for (HMB) to different wave numbers in the complexes in rang (1251-1242) and (1188-1166). Thus, it can be concluded that the ligand act as a bidentate via the hydrazide N and phenolic O atoms. The proposed coordination positions are confirmed by the appearance of new bands at (491-474) cm^{-1} and (515-511) cm^{-1} which are attributed to υ (M-N) and υ (M-O) a respectively [16-19]. Figure 3(a and b) shows the spectra of the prepared compounds

.

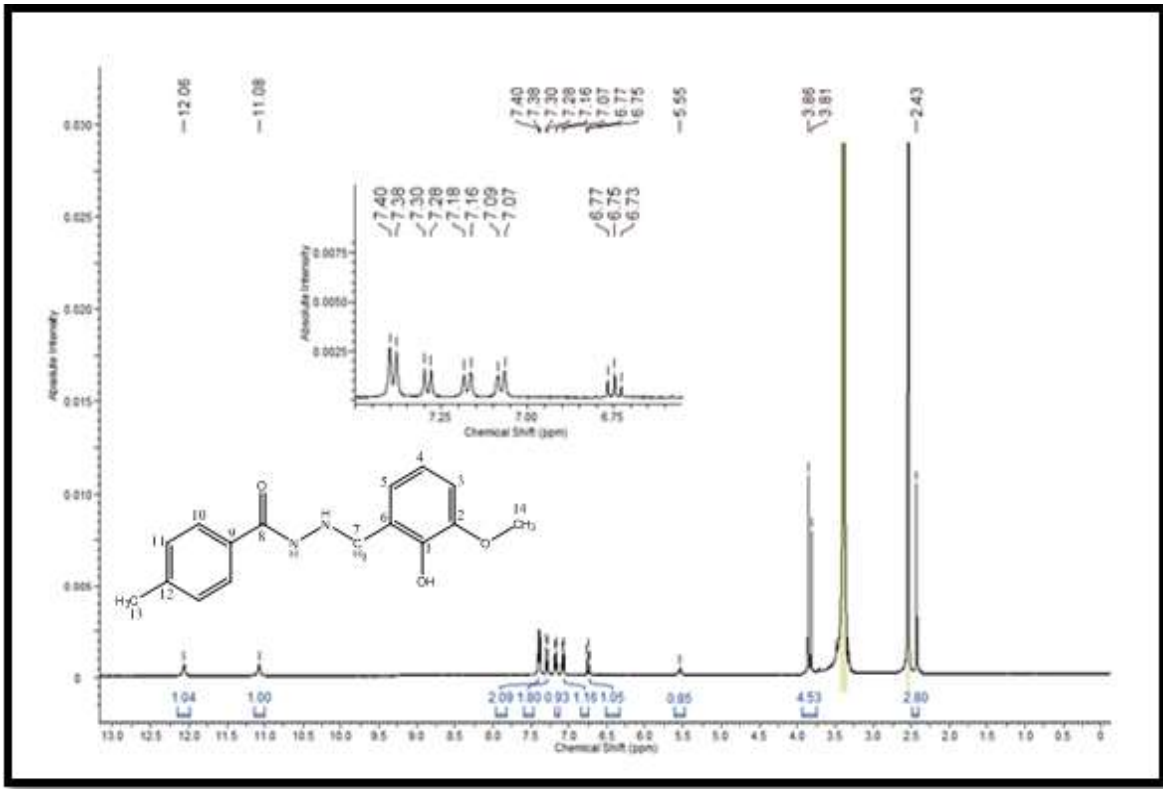

A

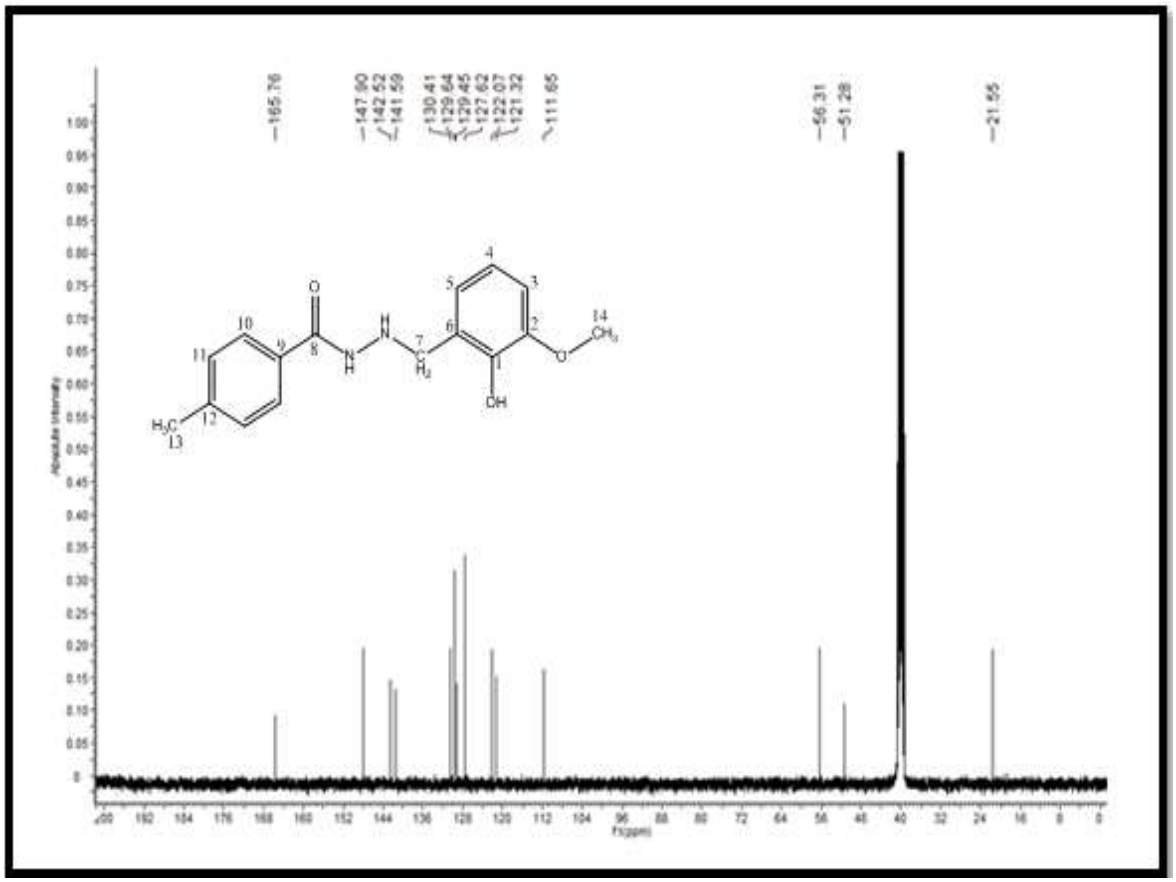

B

Figure 2. A- [1]HNMR Spectra B- [13]CNMR Spectra (b) of ligand (HMB)

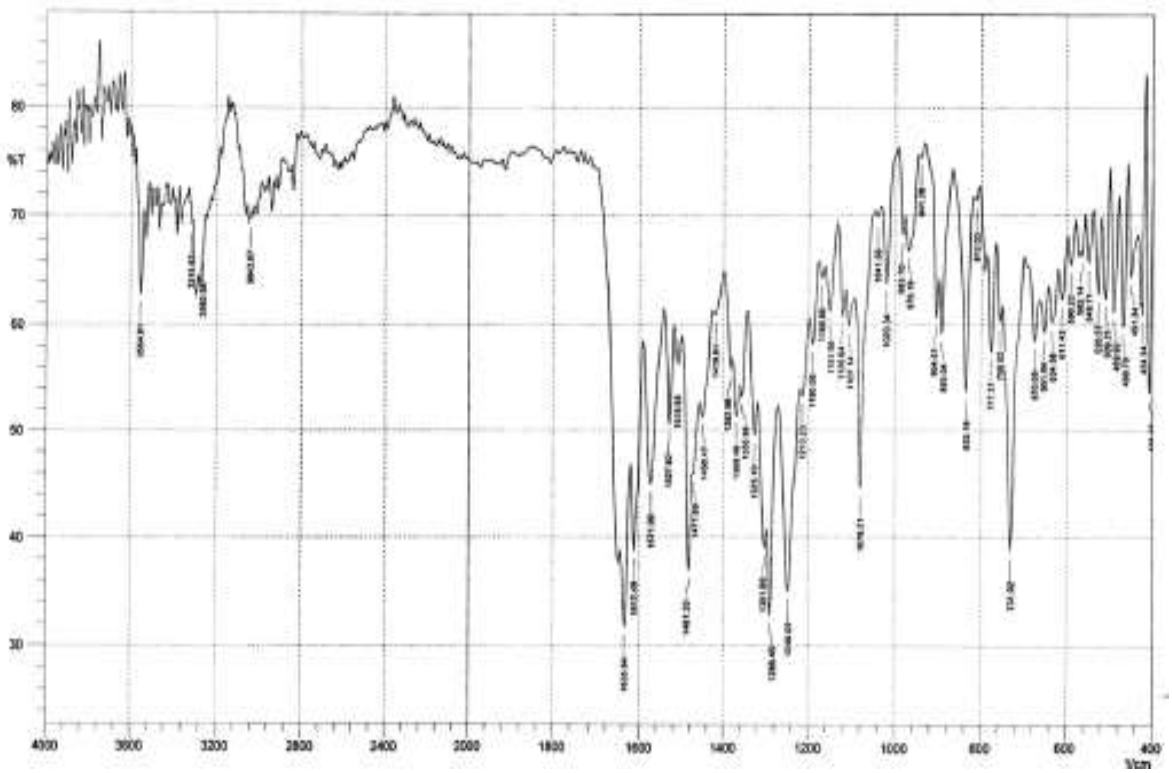

A

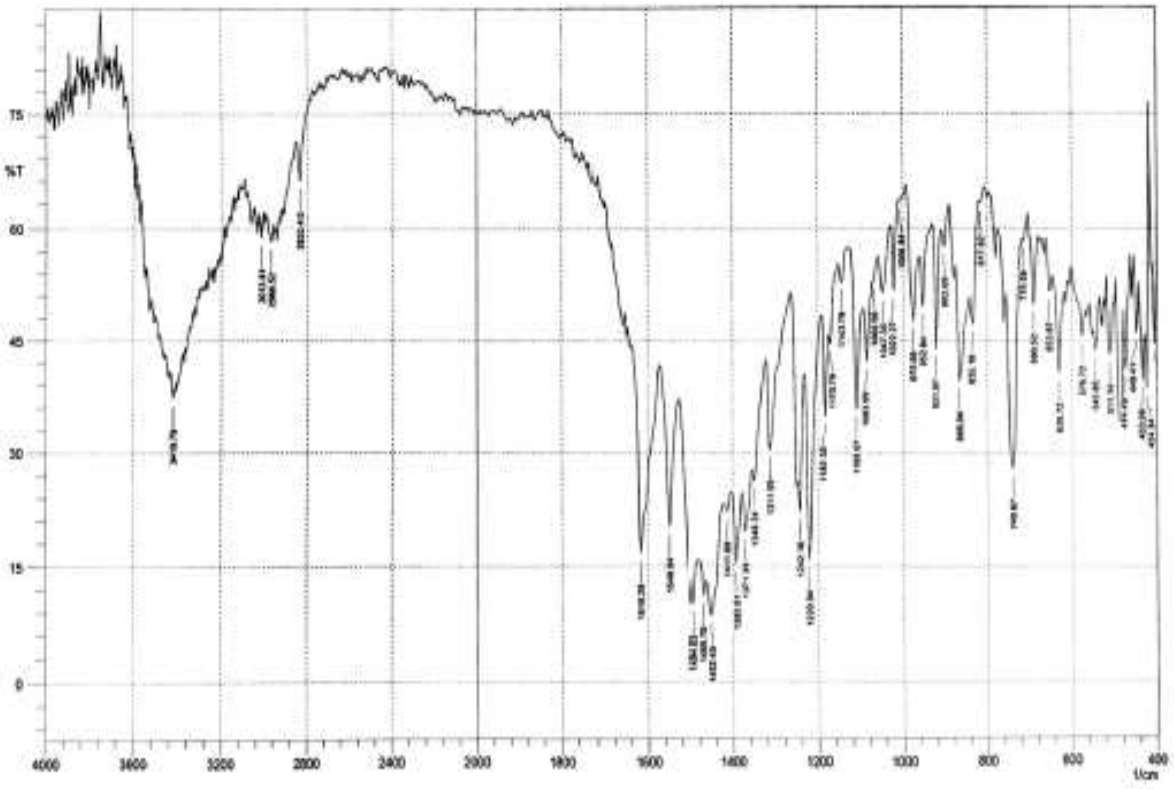

B

Figure 3. FTIR Spectra of ligand A, Vanadyl complex B

Table 2. FT-IR data of HMB and complexes

Com.	υ (N-H) hydrazide	υ (O–H) phenol	υ (C-O) phenol	υ (M-O)	υ (M-N)	υ (V=O)
Ligand (HMB)	3315 3263	34˚4	1246 1190	———	———	———
VO complex	3319	———	1242 1182	511	474	850
Cr complex	3383	———	1247 1188	513	491	———
Cu complex	3364	———	1251 1166	515	489	———

Electronic spectra of prepared compounds are included in the Table 3, Figure 4(a and b).

Electronic spectra of prepared compounds [20-22]

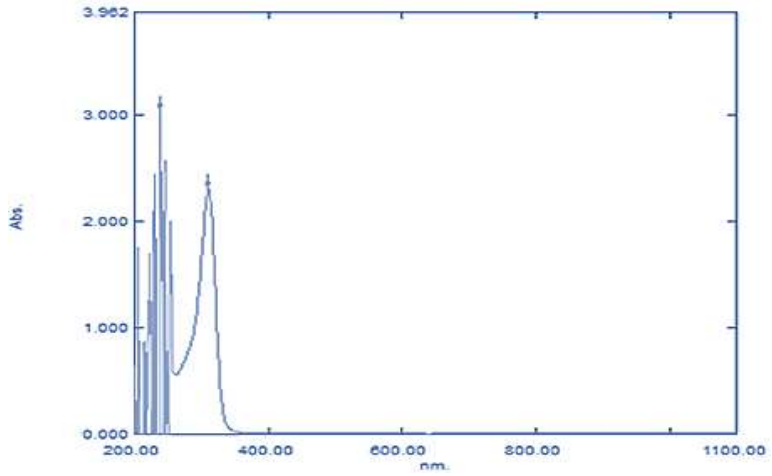

A

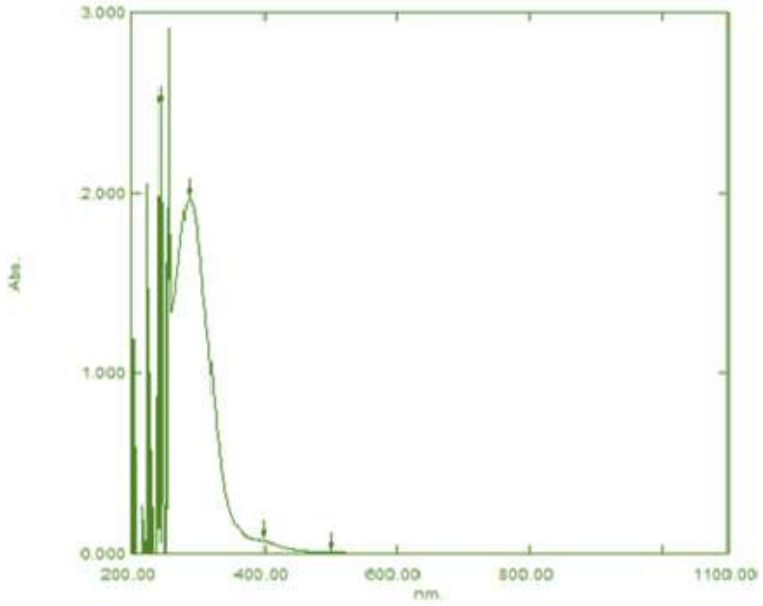

B

Figure 4. Electronic Spectra of ligand (A) and free copper complex (B)

Table 3. Electronic transfer's data of HMB and its complexes

Com.	Wave number		ε_{max} molar^{-1} cm^{-1}	Transitions	Geometric structure	μ_{eff} B.M.	Conductivity $Ohm^{-1}cm^2mol^{-1}$ in (DMSO)
	nm	cm^{-1}					
Ligand (HMB)	238 313	41841 32258	3037 2304	π→π* n→π*	------	------ --	--------
VO complex	280 825	35714 12121	2410 18	Intra Ligand d→d	pyramidal	1.66	20
Cr complex	289 524 577 979	34602 19083 17331 10214	527 42 34 37	Intra Ligand $^4A_2g \rightarrow {}^4T_1g$ (p) $^4A_2g \rightarrow {}^4T_1g$ (f) $^4A_2g \rightarrow {}^4T_2g$ (f)	Octahedral	3.68	17
Cu complex	242 287 400 475	41322 34842 25000 21052	2482 1967 98 110	Intra Ligand Intra Ligand C.T $^2B_1g \rightarrow {}^2Eg$	Square planar	2.06	15

Results of docking study and then discussion[23-25]

The (HMB) ligand is located on a hydrophobic gap in the 2vid protein (gap 2) composed of the beta sheets of and chains. The main forces of this interference, in addition to the van der Waals interactions are the charge transfer interference between the coloring ring and the aromatic ring in Y186 and the hydrogen bonding between the carbonyl group in the ligand and hydroxyl S145, Figure 5(a) and Table 4.

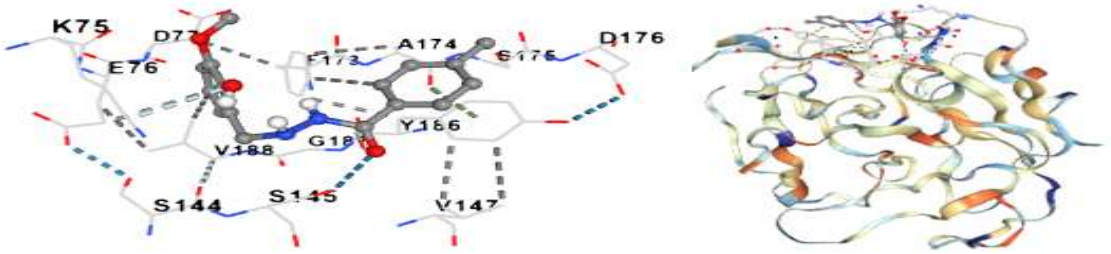

(a)

The second place in the strength of fusion of the (HMB) ligand with the 3vid protein is gap 5 with segments {H39, V40}15, {S23, A24}, and { T152, E153, S154, G155, S157} and {H172, F173, A174, S175}, where the phenolic and etheric oxygen atoms in the ligand interfere with the hydroxyl of the amino acid S175 through hydrogen bonding, as well as a group atom hydrazine with H39 through hydrogen bonding as well ,Figure 5(b) and Table 4.

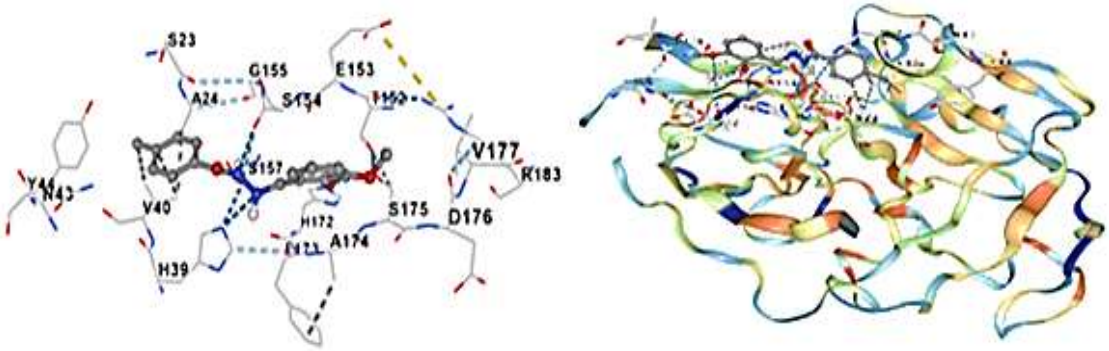

(b)

In the interference of (HMB) ligand with protein 3zmj No. (1), the interference is not on the surface of the protein, but in a large hydrophobic pocket (572 A3) in which four alpha helices form its main structure, where The ligand overlaps {G198, G199, L200, G202, V204, Y205}, {M149, H150, F153, N154}, {G246, M247, M249, H254}, and W236 The basis for the overlap here is van der Waals bonding and the hydrogen bonding between the phenolic OH group of the ligand and the sulfur atom in M249, Figure 5(c) and Table 4.

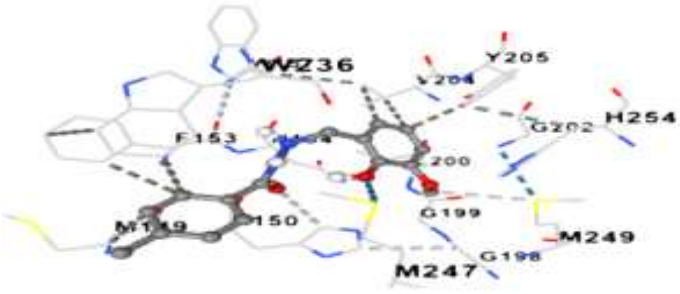

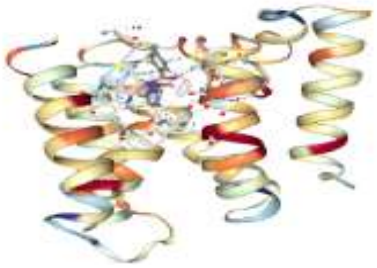

(c)

The other site with the same overlapping strength, but with a smaller gap size is the one with the number 2 in table (4), and it is almost the same as the previous gap, but with a different overlapping position. The overlap segments in this gap are {G246, M247, M249, H254}, {F153, N154, W157}, {M149, H150}, and {G198, G199, L200 , G202, V204, Y205} and W236. The main forces of interference are the van der Waals forces and the hydrogen bonding between the phenolic OH and the sulfur atom in M247 and the carbonyl group and H150, Figure 5(d) and Table 4.

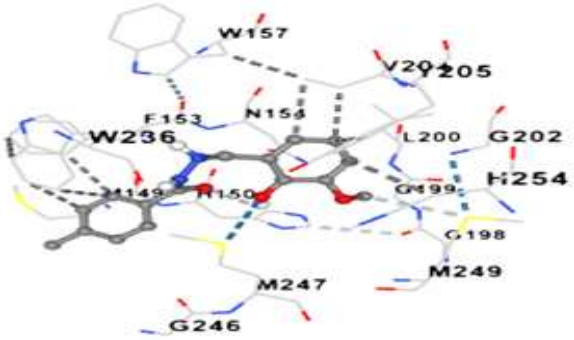

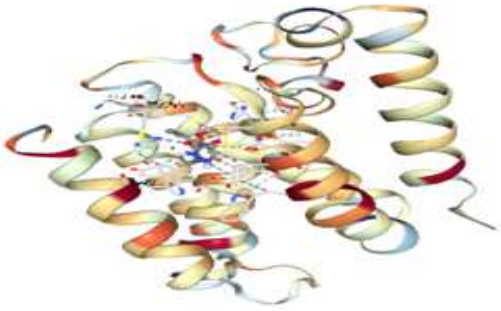

(d)

In the overlap of the cis-[Cu(HMB)$_2$] complex with protein 2vid as shown in Table 4, the highest order gaps of overlap are number 2 and then number 1. In gap number 2 the complex overlaps with the protein Through a hydrophobic pocket in which the beta sheets form the largest side, which is {K75, E76, D77} and {F173, A174, S175, D176, Y186} and {S140, E142, G143, S144, S145, V147}, the following interactions occur interference of the type of charge transfer between the toluene ring in the complex with Y186, in addition to hydrogen bonding between the carbonyl group in the complex and S145, in addition to one of the phenolic oxygens with K75, Figure 5(e) and Table 4.

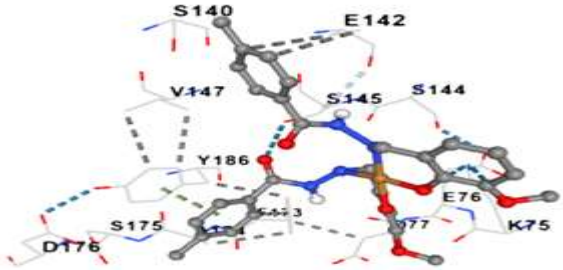

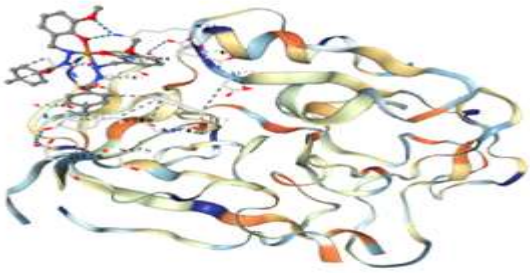

(e)

In second place in the strength of interference is gap No. 1, which is also a hydrophobic gap built-in general from beta sheets for the chains {P92, K93, N98, D99, N100, V101, T102, P103} and {N11, I12, F13, T16}, where F13 interferes with the coloring ring through the transfer of charge and one of the carbonyl groups of the complex with K93 through hydrogen bonding, Figure 5(f) and Table 4.

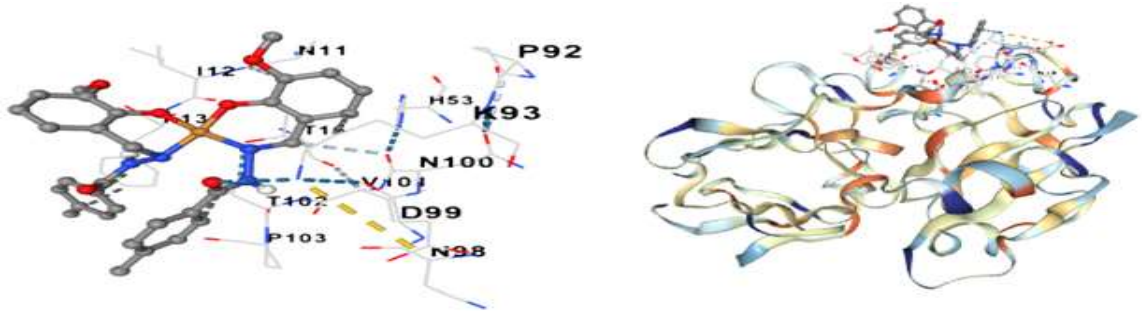

(f)

The cis-[Cu(HMB)$_2$] complexes with the 3zmj protein through hydrophobic vacuole 2 where the following segments co-interlate: {W236, L244, G246, M247, S248} and {F146, S147, M149, H150, F153} And the driving forces for this interference, in addition to the van der Waals forces, are the charge transfer forces between the coloring ring and F146, Figure 5(g) and Table 4.

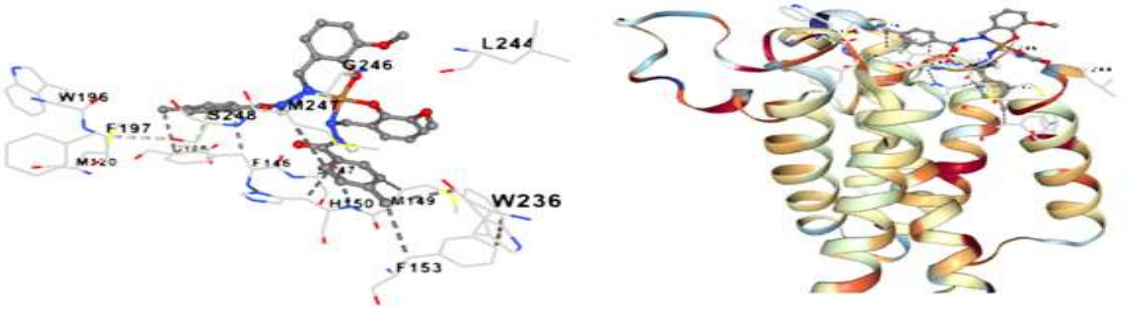

(g)

Next comes Gap 3 in terms of interference strength. So is the case in terms of hydrophobic interference sites. The following segments are co-conjugated with complexes {F135, W136, F139, T140, A142, L143} and {V96, V99, M100, A103, V107} and L123. On these sites there is no room for association other than that of the van der Waals type, Figure 5(h) and Table 4.

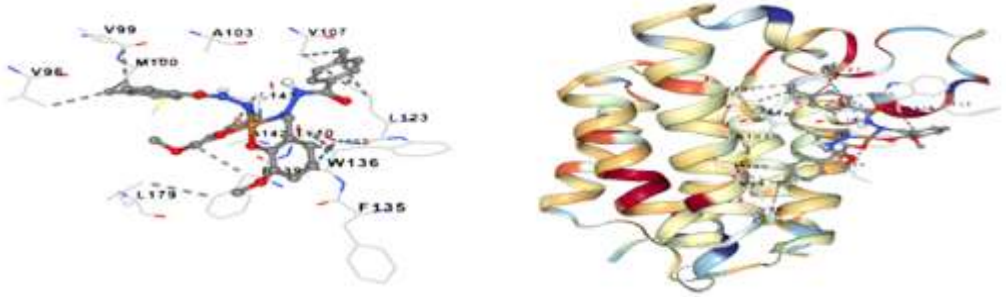

(h)

The tras-[Cu(HMB)$_2$] complex overlaps with the 2vid protein through a hydrophobic pocket in the protein with the highest interference strength with gap number 1 in the table. The complex overlaps with beta sheets through sections {F173, A174, S175, V188}, {K75, E76, D77}, and {K38, H39}, where all the overlaps are of van der Waals type, Figure 5(i) and Table 4.

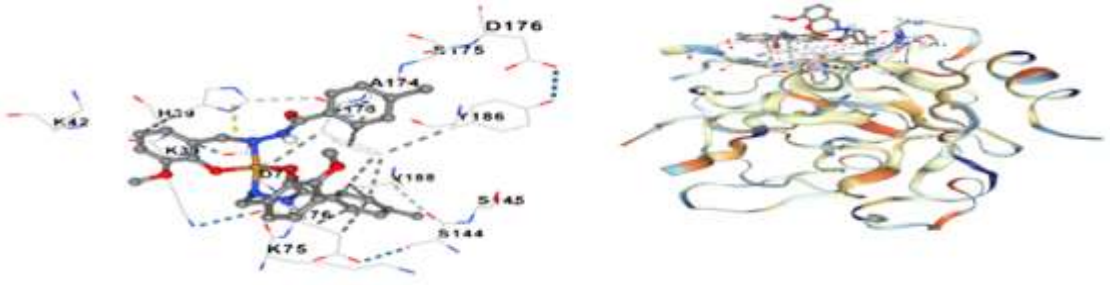

(i)

Divide 2 has the same strength as overlapping, but with smaller cross-sections involved in overlapping with the trans-[Cu(HMB)$_2$] complex, {S154, S157}, {H39, V40}, and {S154, S157}. F173, A174}, A24, and D77 in this site, unlike the previous site, there was a significant network of hydrogen bonds centered on segments S154 and S157 with the carbonyl group and NH groups present in the complex, in addition to the overlap of charge transmission between the aromatic coloring ring of the complex and between sections H39. Due to the strength of the interferences identified in this gap, the size it occupied is smaller than the previous gap, which did not include specialized strong interferences, Figure 5(j) and Table 4.

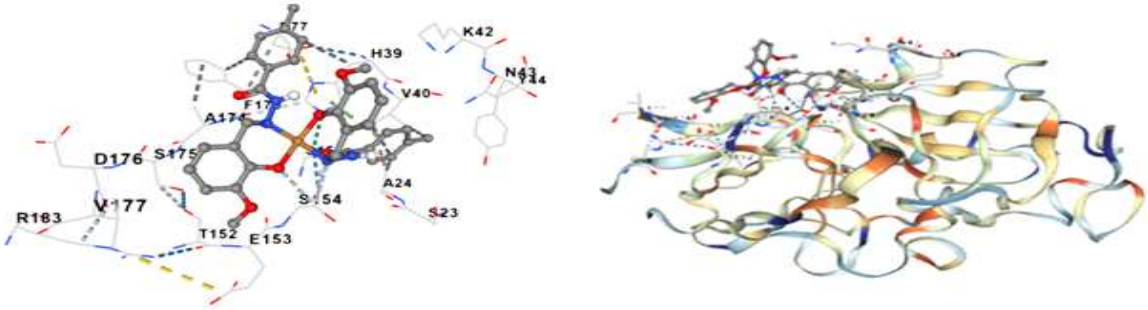

(j)

In the overlap of the [Cu(HMB)$_2$] complex with the 3zmj protein in gap 3, the complex is positioned between a group of alpha helices with segments {P95, V96, V99, M100, A103} and {F135, W136, F139, T140, A142, L143} and {T178, L179, A182}, as the interferences that occurred are of the Van der Waals type, in addition to the interference of charge transfer between the aromatic coloring ring and the segment F139, Figure 5(k) and Table 4.

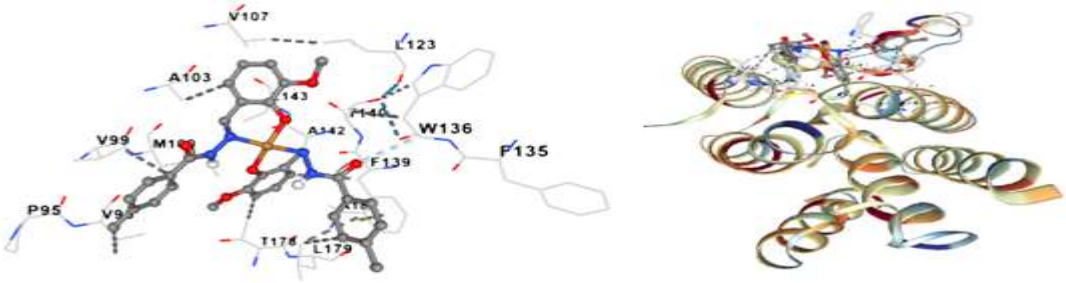

(k)

The trans-[Cu(HMB)$_2$] complex interferes with the 3zmj protein in gap 5 by positioning between alpha helices with segments {V105, F108, I109, Q112, I113} and { L148, I151, L152, L155} where all interference forces are van der Waals ,Figure 5(l) and Table 4.

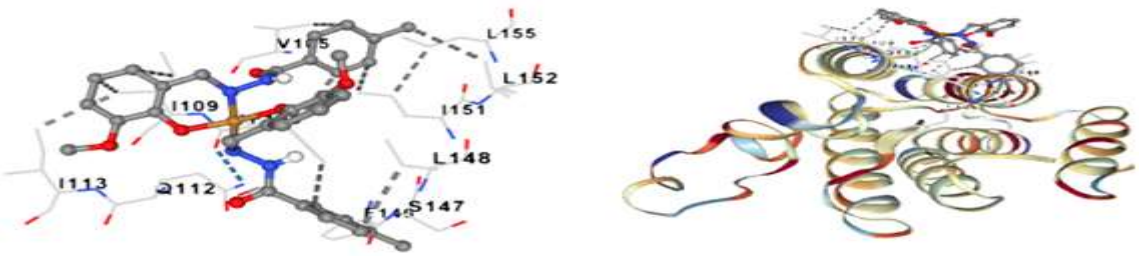

(l)

Figure 5(a-l). The binding of the (HMB) ligand and its copper complex within the active site of the enzyme and shows the number and type of hydrogen bonding of the different positions with the amino acids of the active site.

Table 4 . Orders and overlap centers for the molecular docking process of ligand (HMB) and its square planar copper complex of both type's cis and trans with 2vid and 3zmj proteins

Cavities Ligand (HMB) + 2vid	**volume**	**center_x**	**center_y**	**center_z**	**size_x**	**size_y**	**size_z**	**score (kcal/mole)**
1	148	29.33	38.323	29.204	23	23	23	-5.6
2	105	22.677	24.809	2.994	23	23	23	-6.6
3	102	31.298	43.833	10.465	23	23	23	-6
4	87	25.178	21.04	20.62	23	23	23	-5.9
5	68	33.927	37.079	7.134	23	23	23	-6.3
Cavities Ligand (HMB) + 3zmj	**volume**	**center_x**	**center_y**	**center_z**	**size_x**	**size_y**	**size_z**	**score (kcal/mole)**
1	572	-11.371	-7.165	50.643	23	23	23	-7.5
2	191	-9.243	-11.579	56.151	23	23	23	-7.5
3	138	-25.209	-2.806	41.799	23	23	23	-5.8
4	104	-8.016	-8.238	30.82	23	23	23	-6.3
5	103	-11.125	5.184	45.728	23	23	23	-6.5
Cavities cis-Cu complex + 2vid	**volume**	**center_x**	**center_y**	**center_z**	**size_x**	**size_y**	**size_z**	**score (kcal/mole)**
1	148	29.33	38.323	29.204	25	25	25	-7.7
2	105	22.677	24.809	2.994	25	25	25	-8.3
3	102	31.298	43.833	10.465	25	25	25	-7
4	87	25.178	21.04	20.62	25	25	25	-7.6
5	68	33.927	37.079	7.134	25	25	25	-6.9
Cavities cis-Cu complex + 3zmj	**volume**	**center_x**	**center_y**	**center_z**	**size_x**	**size_y**	**size_z**	**score (kcal/mole)**
1	572	-11.371	-7.165	50.643	25	25	25	-7.7
2	191	-9.243	-11.579	56.151	25	25	25	-8.8
3	138	-25.209	-2.806	41.799	25	25	25	-8.5
4	104	-8.016	-8.238	30.82	25	25	25	-7.9
5	103	-11.125	5.184	45.728	25	25	25	-7.8
Cavities trans-Cu complex + 2vid	**volume**	**center_x**	**center_y**	**center_z**	**size_x**	**size_y**	**size_z**	**score (kcal/mole)**
1	148	29.33	38.323	29.204	24	24	24	-7.5
2	105	22.677	24.809	2.994	24	24	24	-7.5
3	102	31.298	43.833	10.465	24	24	24	-6.2
4	87	25.178	21.04	20.62	24	24	24	-7
5	68	33.927	37.079	7.134	24	24	24	-7.5
Cavities trans-Cu complex + 3zmj	**volume**	**center_x**	**center_y**	**center_z**	**size_x**	**size_y**	**size_z**	**score (kcal/mole)**
1	572	-11.371	-7.165	50.643	24	24	24	-6.8
2	191	-9.243	-11.579	56.151	24	24	24	-6.6
3	138	-25.209	-2.806	41.799	24	24	24	-8.6
4	104	-8.016	-8.238	30.82	24	24	24	-6.8
5	103	-11.125	5.184	45.728	24	24	24	-7.6

Results of Density functional theory (DFT) and then discussion

Ligand (HMB) and its complex with copper cis-$Cu(HMB)_2$ and trans-$Cu(HMB)_2$ were constructed by Gauss view 5 interface and performing the calculations in the Gaussian 9 program[26].

In the beginning, Geometry Optimization was done for ligand and complex according to semi-empirical methods and the PM6 function within restricted spin conditions for ligand and unrestricted spin conditions for complex until a stable geometry is reached. An additional Geometry Optimization process was performed after changing the calculation method to unrestricted DFT with a basis function of Lanl2dz and using the Exchange Correlation Potential B3-LYP in the case of complex and restricted DFT and with a basis function of 3-21 G with the same Exchange correlation potential used for complex. Upon reaching the stable geometry of the molecule, the state energy was calculated according to the last calculation settings for ligand and complex.

In the geometry of the ligand (HMB), we note that the group (C=O) -NH-NH is located outside the plane of the aromatic ring attached to the N atom because of the presence of the separating homologous group. Therefore, the largest electronic interference of this group occurs with the associated aromatic ring with the carbonyl group, and this group tends to hydrogen bond between the O atom in the CO group and the NH proton attached to the methyl group, Figures 6-8.

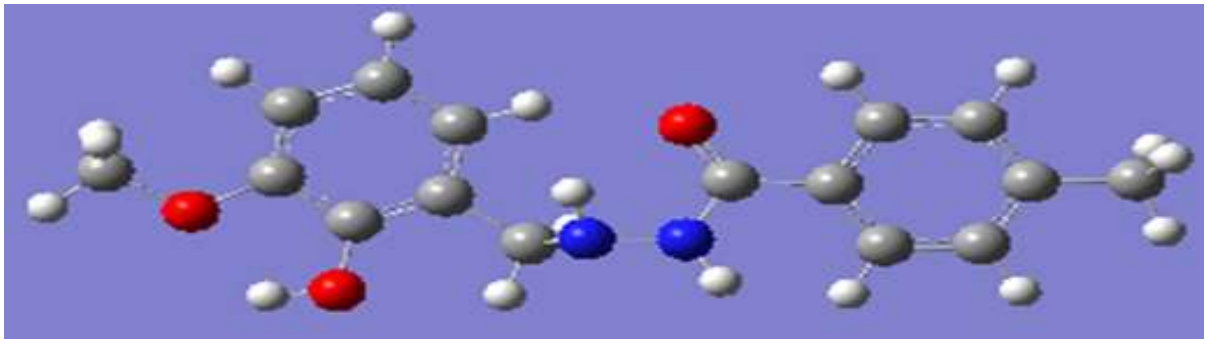

Figure 6. Structure of ligand (HMB)

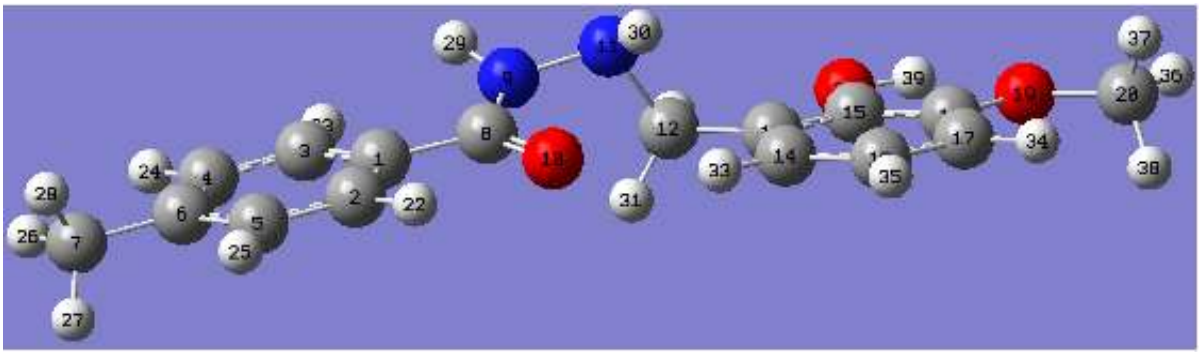

Figure 7. Structure of ligand (HMB) after Geometry Optimization

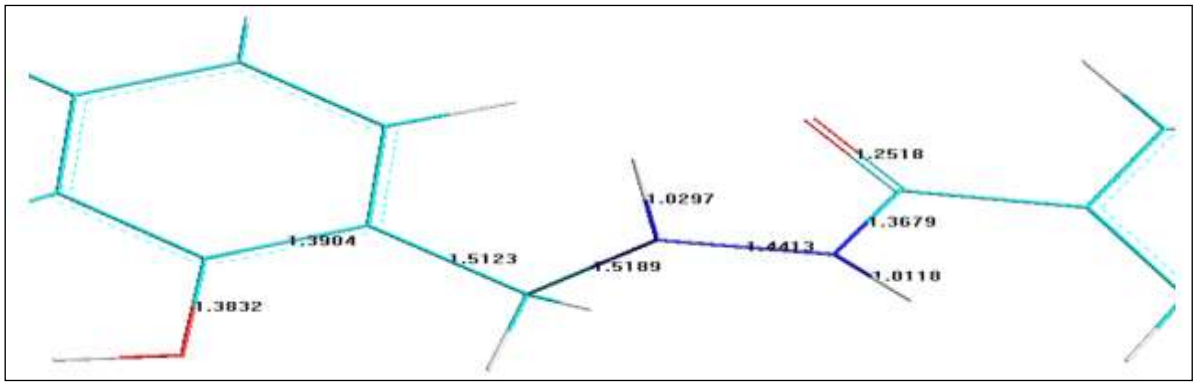

Figure 8. The lengths of the links involved in the coordination band in the ligand (HMB)

In the cis-$Cu(HMB)_2$ complex, we find that the geometry of the complex as a whole moves away from taking the planar position due to the large size of the ligand, which leads to a state of

steric crowding around the central ion with the preservation of the internal structure of the center of coordination in the form of a flat square, the group (C=O)-NH-NH, which has become adjacent to the center of symmetry. We note that one of its two groups retains a geometry that allows the implicit hydrogen bonding that was mentioned earlier to remain, but for the other group, internal rotation of dihedral angles occurs in which this does not remain with it. Hydrogen interference, and instead, an opportunity is generated for hydrogen interference between the proton in it and the N atom in the corresponding group, Figure 9,10.

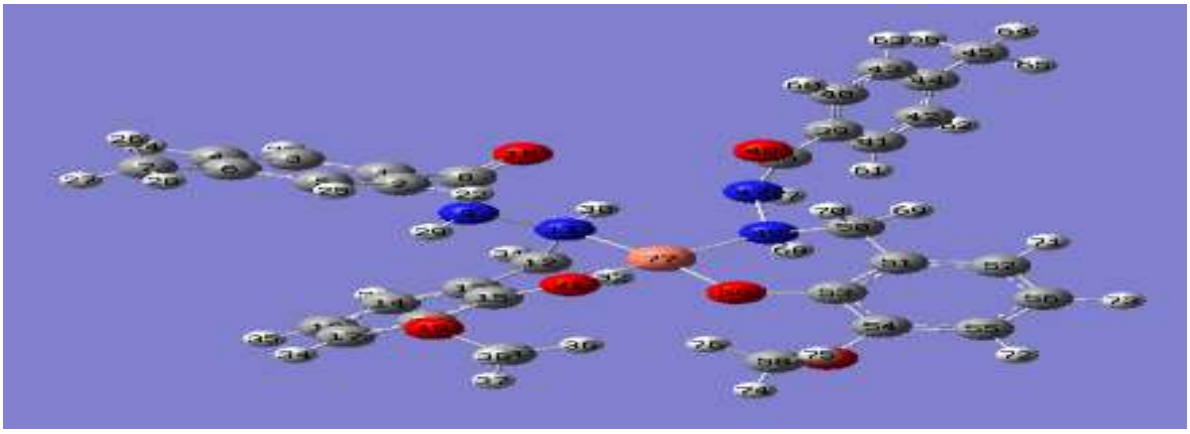

Figure 9. Structure of the cis-Cu(HMB)$_2$ complex after Geometry Optimization

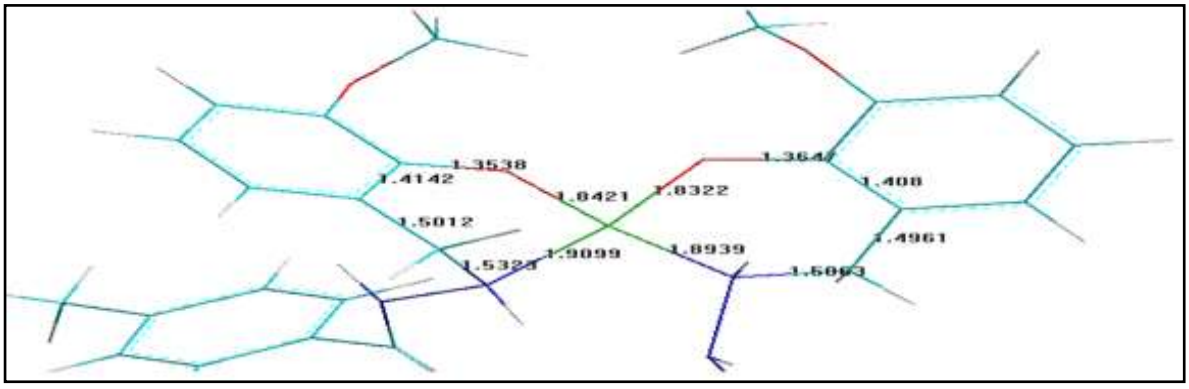

Figure 10. The lengths of the bonds in the center of coordination of the cis-Cu(HMB) complex

In the complex trans-Cu(HMB)$_2$,we notice the same general deviation from the planar structure with respect to the molecule as a whole, while remaining with respect to the center of coordination as before. The internal hydrogen bonding in the group (C=O) -NH-NH[(27)] is completely broken and replaced by other hydrogen bonding between the NH protons coordinated with the central ion and the phenolic O atoms bonded to the copper ion, forming two structures of the four rings of hydrogen bonding is adjacent to the square of symmetry, Figure 11,12.

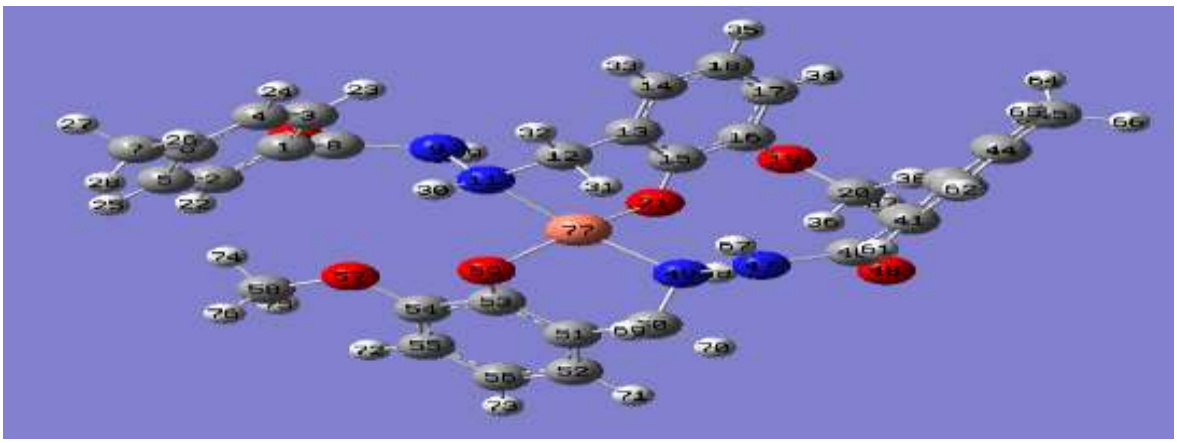

Figure 11. Structure of the trans-Cu(HMB) complex after Geometry Optimization

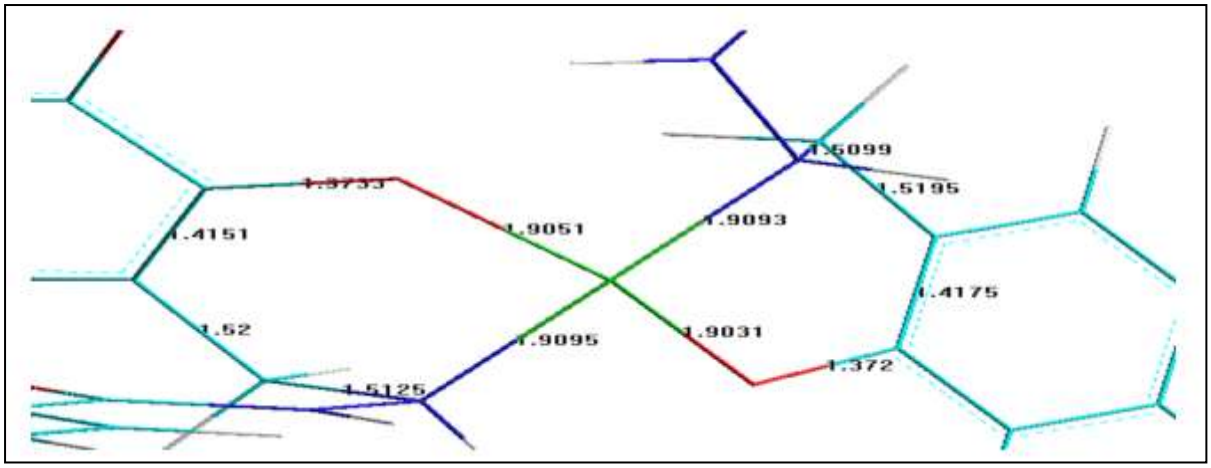

Figure 12. The lengths of the bonds in the center of coordination of the trans-Cu(HMB) complex

In the ligand (HMB), we notice the centering of the HOMO orbital on the phenolic hydroxyl group with the aromatic ring that carries it, and this represents one of the factors that contributed to making this group one of the coordination centers with the copper ion, as is the case for the N atom associated with a group The two homologs contributes a percentage of the HOMO orbital concentration, but to a lesser extent than in the case of the hydroxyl group, so this atom was the second point of bonding in the formation of complexes with the copper ion. In the LUMO orbital of the ligand (HMB), we notice that this orbital is centered on the aromatic ring, not far from the bonding center with copper. On this basis, the formation of the complex of copper with the ligand (HMB) contributes to increasing stability by reducing the transmission voltage barrier. The charge between the two aromatic rings in the ligand (HMB), which is expressed by the function Eg in Table 5.

In complexes of copper with ligand (HMB), we find that the copper ion worked to increase the concentration of the HOMO orbital on the aromatic ring system that carries the hydroxyl group and the stability of the LUMO orbital on the coloring ring, Figure 13-15.

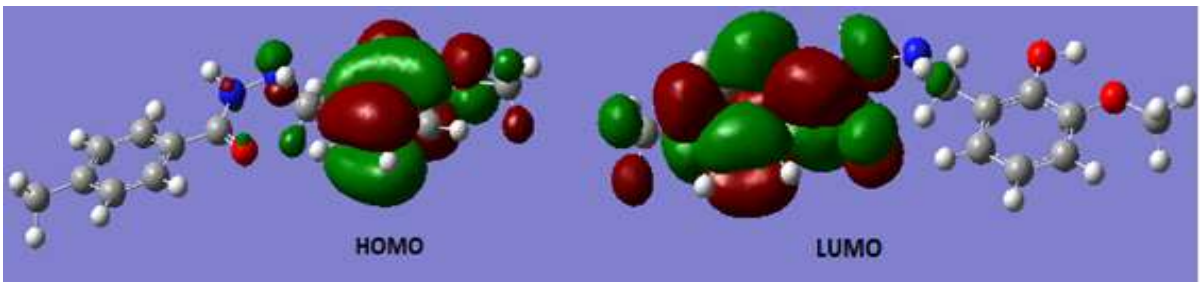

Figure 13. The energy levels of the ligand (HMB)

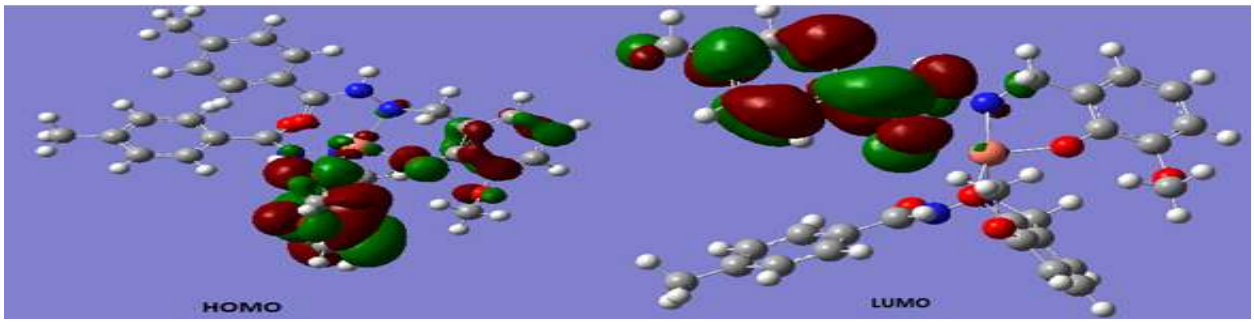

Figure 14. The energy levels of the cis-Cu(HMB) complex

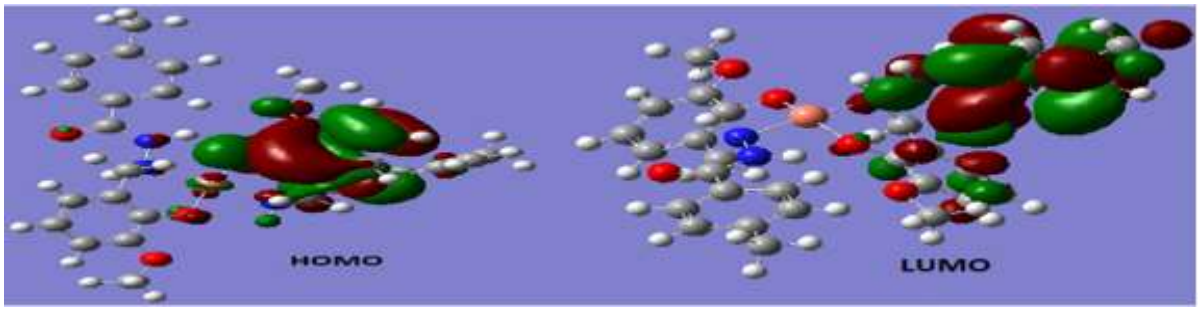

Figure 15. The energy levels of the trans-Cu(HMB) complex

Table 5. The values of energy levels (LUMO and HOMO), in addition to the functions derived from them, for each of the ligand and complexes

compound	Method	HOMO (H)		HOMO average (H)	LUMO (H)		LUMO average (H)
		α	B		α	β	
Ligand (HMB)	3-21G-B3LYP	-0.198		-0.198	-0.033		-0.033
cis-Cu complex	u-lanl2dz-b3lyp	-0.188	-0.185	-0.187	-0.118	-0.117	-0.117
trans-Cu complex	u-lanl2dz-b3lyp	-0.166	-0.165	-0.165	-0.051	-0.077	-0.064
Compound	**Eg (energy gap) (H)**	**μ electronic chemical potential (H)**	**χ (electro-negativity) (H)**	**H (hardness) (H)**	**σ global softness (H)**	**ω (electro-phlilicity index) (H)**	**Nu Nucleophilicity Index (H)**
Ligand (HMB)	0.165	0.115	-0.115	0.115	8.667	0.058	17.334
cis-Cu complex	0.069	0.152	-0.152	0.152	6.576	0.076	13.152
trans-Cu complex	0.101	0.114	-0.114	0.114	8.734	0.057	17.468

From the values of the energy levels of the orbitals LUMO and HOMO, the energy gap (Eg), the electrochemical potential (μ), the electronegativity (χ), and the hardness (η) were calculated, as were ductility (σ), electrophilicity criterion (ω), and the nucleophilic criterion (Nu) from the following equations:

$$E_g = E_{LUMO} - E_{HOMO} \dots\dots\dots\dots (1)$$

$$\mu = \frac{E_{LUMO} + E_{HOMO}}{2} \dots\dots\dots\dots (2)$$

$$\chi = -\mu = \frac{-(E_{LUMO} + E_{HOMO})}{2} \dots\dots\dots\dots (3)$$

$$\eta = \frac{-(E_{LUMO} - E_{HOMO})}{2} \dots\dots\dots\dots (4)$$

$$\sigma = \frac{1}{\eta} \dots\dots\dots\dots\dots\dots (5)$$

$$\omega = \frac{\mu^2}{2\eta} \dots\dots\dots\dots\dots\dots\dots (6)$$

$$Nu = \frac{1}{\omega} \dots\dots\dots\dots\dots\dots (7)$$

The chemical potential is a measure of the stability of the molecule, where we find an increase in the stability of the complexes compared to the ligand from which they came, with a significant decrease in the chemical potential of the trans-Cu(HMB) complex compared with the cis-Cu(HMB) complex. In association with a high nucleophile value close to the nucleophile value of the original ligand. It is likely that the reason for this behavior may be due to the fact that in the cis-Cu(HMB) complex, the arrangement of the two adjacent electrophilic carbonyl groups works to increase the strength of the electrophilic field of the molecule as a whole through polarization, and decreasing the value of its nucleophile and increasing its stability, unlike what it is. This is the trans-Cu(HMB) complex[28, 29].

Results of Biological studies of the cupper complex (Anticancer study and Antibacterial)

Anticancer Study

The IC_{50} method, which estimates the concentration of a medication that inhibits cell lineout growth by 50%, was used to evaluate the anticancer and growth-inhibitory effects. Compounds suffering IC_{50} values less than 5.00 μg/ml, between 5.00 and 10.00 μg / ml, and

between 10.00 and 25.00 µg / ml, respectively, are regarded as having strong, moderate, and mild anticancer activity.

The Cu complex demonstrated robust anticancer activity with an IC50 of (3.349 µg /ml), whereas the HMB ligand demonstrated modest antitumor activity with an IC_{50} of 22.75 µg/ml, Figure16. The results indicate that the Cu complex obtained is more efficient than the ligand.

The results showed that the nature of the chemical groups present within the compounds has a major role in determining the effectiveness of these compounds. If the group is basic, these compounds have high toxicity against HepG2 cells compered to regular cells line, making them very efficient in restricting disease dissemination. Because normal and cancerous cell lines differ in their receptors, the toxicity of cancer cells varies from one cell line to another.

It was noted that the amide group has the potential to act as an inhibitor of cancer cells by affecting certain receptors on the surfaces of these cells. Through these receptors, the cells surrender to programmed death. The data showed that both the concentration and type of compound used are important in determining the amount of cytostatic failure.

The inhibition rate of cell growth in normal and cancerous lines increased when the concentration of copper (ll) complexes was increased, and this phenomenon is known as (dose-dependent).

The finding revealed that the form of the compound has an impact on the rate at which cancerous and normal cell lines are inhibited from growing, with strong variations between the two complexes as seen in Table 6, where it was found that the complexes have an effect on the growth of cancerous and normal lines cells with the same concentration and duration Exposure, we notice that the copper complex has a toxic effect against cancer cells of HepG2 cells, because copper is an important mineral in the work of anti-toxic enzymes, i.e. it acts as an enzyme companion necessary for the work of the enzyme. It was a SOD enzyme (Superoxide dismutase), Which works to convert oxygen (O_2) to H_2O_2 and then it turns into H2O and through the action of enzymes catalase that work to remove the toxicity of free radicals formed from an internal source (mitochondria) or an external source and the meaning of the enzyme's action is the station of the electron transport chain, In the mitochondria, which generates ATP Copper inhibits oxidative phosphorylation in cancer cells, according to this study[30, 31], as illustrated in Table 6 .According to all this resulted treatments significantly ($p \leq 0.01$) raised the nuclear intensity and Cu-ligand significantly reduced and digesting cancer cell

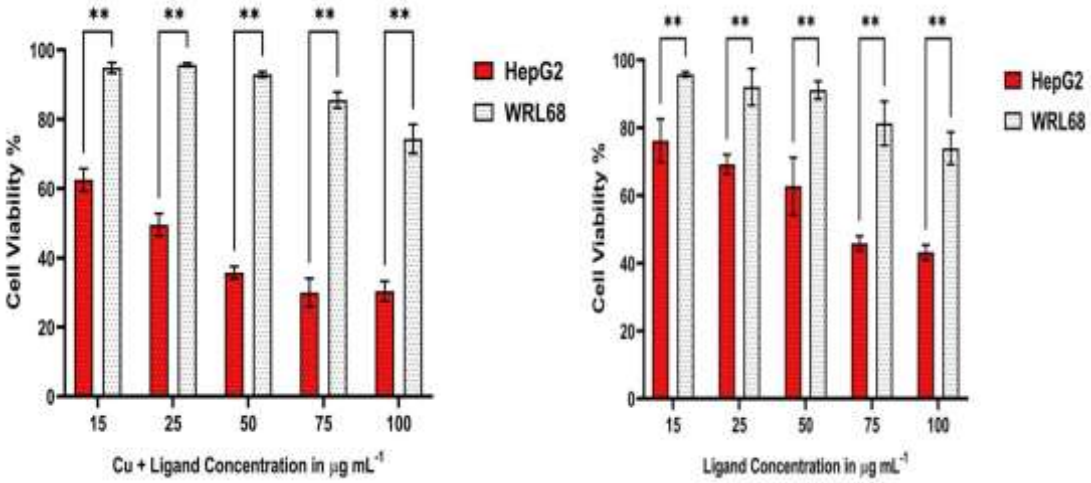

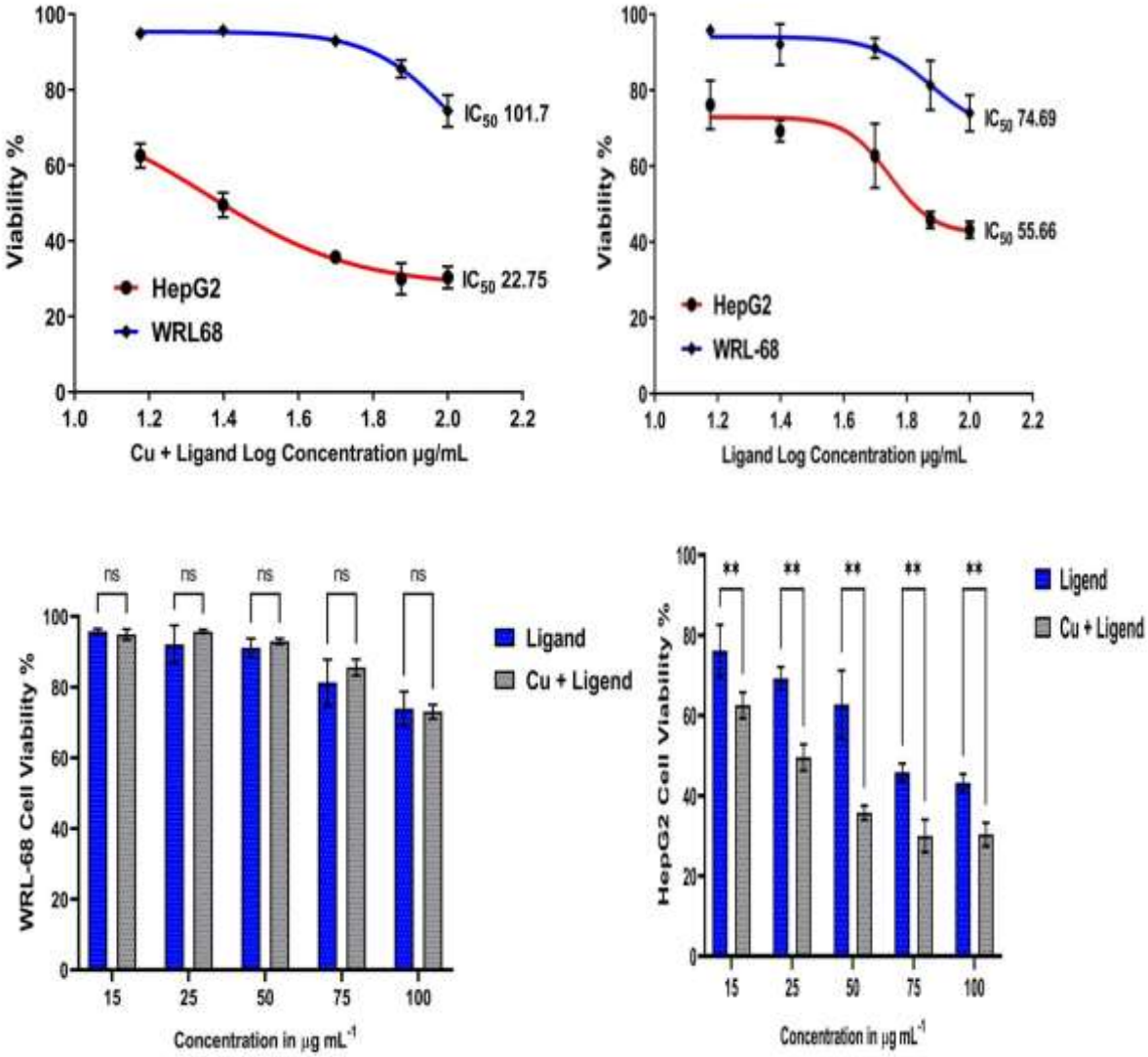

Figure 16. Study of the effect of ligand and copper complex on (HepG2) and (WRL-68)

Table 6 . Study of the effect of ligand and copper complex on (HepG2) and (WRL-68)

	Ligand				**Cu-complex**			
	HepG2		WRL		HepG2		WRL	
	IC_{50} µg mL^{-1}		IC_{50} µg mL^{-1}		IC_{50} µg mL^{-1}		IC_{50} µg mL^{-1}	
	55.66		74.69		22.75		101.7	
Concentrations	Mean	SD	Mean	SD	Mean	SD	Mean	SD
15	76.19	±6.42	95.79	±0.71	62.58	±3.22	94.91	±1.51
25	69.24	±2.87	92.08	±5.41	49.54	±3.26	95.72	±0.53
50	62.75	±8.48	91.13	±2.61	35.76	±1.75	92.94	±0.81
75	45.86	±2.21	81.30	±6.52	29.98	±4.11	85.57	±2.34
100	43.21	±2.20	73.94	±4.78	30.37	±2.88	74.38	±4.21

Significant, $P=\leq 0.01$, SD:Standard Deviation, (n=3)

Antibacterial Study

Preliminary screening was conducted to identify potent antagonistic bacteria toward metal complex. Bacterial isolates towards. As a result of the effect of metal ions on natural cell bacteria, biological activities showed success for the activity of metal complexes. These isolates showed clear growth inhibition in double culture measurements, we followed this method instead of used MIC due to results from MIC studies must be evaluated in

the appropriate context. In the tube corresponding to the MIC, microorganisms were merely prevented from growing and not necessarily killed. Where radioactive inhibition appeared within the range (2-18mm). The reason for the high laboratory effectiveness of the complexes compared to the ligand is that the chelation process significantly reduces the polarity of the metal ion due to the possibility of canceling the position that was associated with the p-electron in the entire ring system that was created throughout the coordination period, in addition to the partial participation related to the positive charge for metals with donor atoms.

Regarding complexes, this chelation causes an improvement in the lipophilic nature with respect to the central metal atom, which leads to an increase in the hydrophobic nature as well as its solubility in fats and then its permeation through the lipid layer of the cell membrane. This process can enhance the rate of entry and absorption and, thus the antimicrobial activities of the tested compounds.

It is clear from this that the antimicrobial activity of metal complexes causes an increase in lipophilicity, and this leads to the disruption of enzymes related to respiratory processes and other cellular enzymes that are important in the metabolic pathways related to the tested microbes (living organisms). Focused on the copper complex because it is more active against the selected bacteria compared to other compounds [32-34], Figure 17,18 and Table 7.

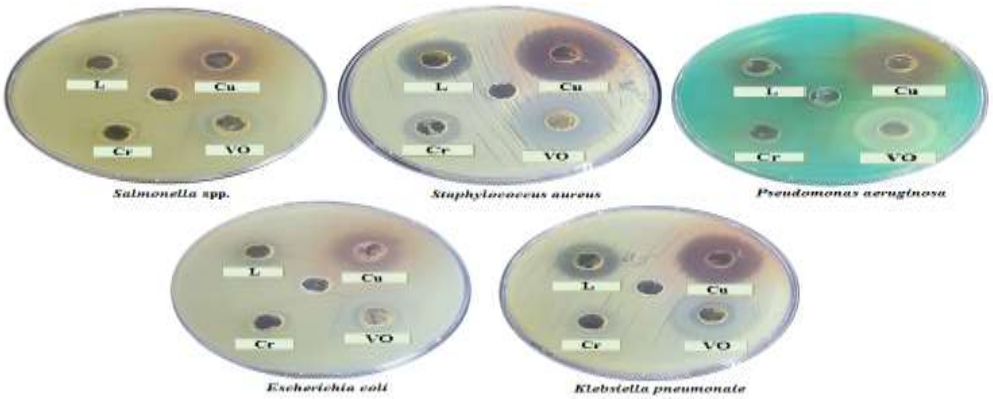

Figure 17. Antibacterial activity of compounds

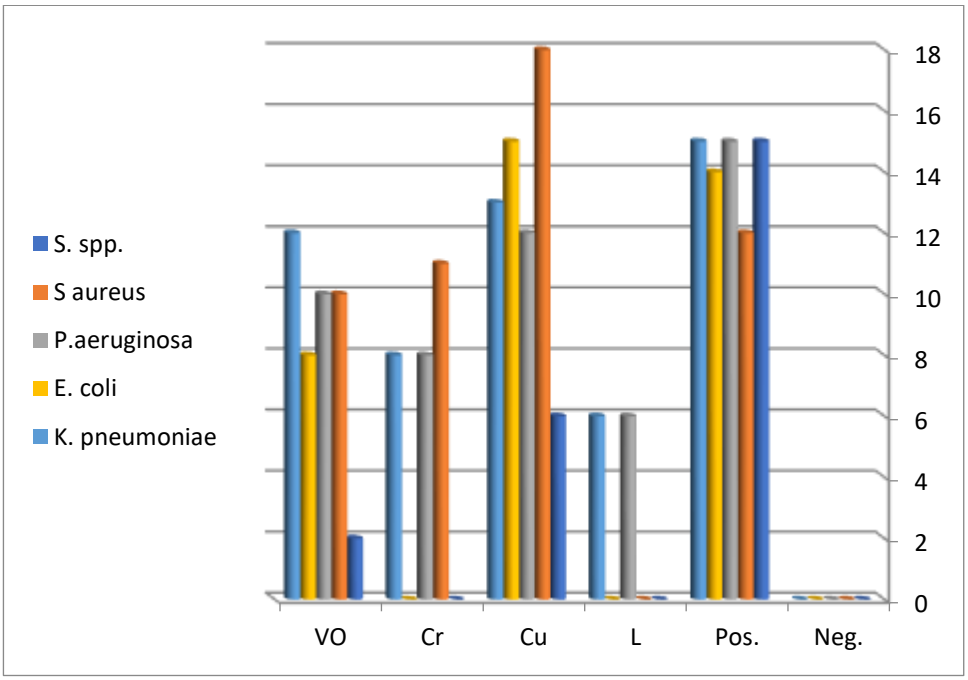

Figure 18. Effect of prepared compounds on selected bacteria

Table 7. Inhibition zone diameter of compounds

Sym.	Com.	Inhibition zone diameter (mm)				
		Salmonella spp.	***Staphylococcus aureus***	***Pseudomonas aeruginosa***	***Escherichia coli***	***Klebsiella pneumoniae***
Neg.	DMSO (Negative control)	0	0	0	0	0
Pos.	Tetracycline (Positive control)	15	12	15	14	14
L	Ligand	0	0	6	0	6
Cu	Cu complex	6	18	12	15	13
Cr	Cr complex	0	11	8	0	8
VO	VO complex	2	10	10	8	12

Conclusion

In this investigation, a novel ligand was synthesized from 4-methylbenzohydrazide and 2-hydroxy-3-methoxybenzaldehyde and coordinated with VO(II), Cr(II), and Cu(II) to form new complexes that were characterized through various physicochemical and spectral investigations. The theoretical study's findings concur with the results from the experiments. Antitumor research on ligand and Cu complex revealed repression of the HepG2 cell line and superior antitumor activity of Cu-complex over ligand. Furthermore, a molecular docking investigation demonstrated that the Cu-complex has the highest possible activity versus *Staphylococcus aureus* and *Escherichia coli*. The bacterial activity of the ligand and its metal complexes was examined against five specific types of bacteria, as the data explained that the activity of the prepared complexes was higher than that of the free ligand, and in addition to that the copper complex showed a good activity against two types of bacteria compared to the other three types. Through density functional theory (DFT) confirming the structure of the composite, the geometry of the copper composite was optimized.

Acknowledgment

As a result of the excellent research support, the author would like to thank the Dean of the College, the Head of the Department, and the workers in the scientific laboratories.

Conflicts of Interest

- Conflicts of Interest: None.
- We hereby confirm that all the Figures and Tables in the manuscript are mine ours.

Funding

The research did not receive any financial funding from any institution.

Ethics Statements

Ethical Clearance: The project was approved by the local ethical committee in University of Baghdad

Author Contribution

Propose a work project, collect sources supporting the idea, begin work, conduct the required measurements, analyze and interpret the results, and approve the final form of the research: **Enass J. Waheed**

References

1. Alhashimy H, Abbas SA. Correlation between Trace Element Levels in Iraqi Breast Cancer Patients. IJPS. 2023; 32(2): 58-64.

2. Mahmood TS, Numan AT, Waheed EJ. Synthesis, spectroscopic identification and antimicrobial activity of mixed ligand complexes of new ligand [3-((4-acetyl phenyl) amino)-5, 5-dimethylcyclohex-2-en-1-one](Hl*) with 3-amino phenol. Biochem Cell Arch. 2020; 20(1): 2235-2245.

3. Shnaikat WN, Al-Khateeb EH, Numan NA, Abbas MM, Shakya AK. Cytotoxic Evaluation of Doxorubicin Combination with Baicalein and Resveratrol Against Hct116 and Hepg2 Cancer Cell. IJPS. 2022; 31: 92-99.

4. Kumari SS. Synthesis, Characterization and Antimicrobial Studies of Metal Complexes from 2-Hydroxy-3-Methoxy Benzaldehyde and L-Serine. Int J Eng Res Technol. 2020; 9(1): 371-375.

5. Claudel M, Schwarte JV, Fromm KM. New antimicrobial strategies based on metal complexes. Chemistry. 2020; 2(4): 849-899.

6. Ji P, Wang P, Chen H, Xu Y, Ge J, Tian Z, et al. Potential of Copper and Copper Compounds for Anticancer Applications. Pharmaceuticals. 2023; 16(2): 234.

7. Hussein RK, El-Khayatt AM, Al Duaij OK, Alkaoud AM. Studying the Biological Activity of Trans-[Cu $(quin)_2(EtOH)_2$] as Potent Antimicrobial Cu(II) Complex through Computational Investigations: DFT, ADMET and Molecular Docking. Front. Biosci. (Landmark Ed). 2023; 28(4): 84.

8. Abdulrahman WA, Othman IA, Waheed EJ. Metal Complexes of Ligand Derived from Amine Compound: Formation, Spectral Characterization, and Biological Evaluation. Int J Drug Deliv Technol. 2021; 11(3): 728-734.

9. Rao VK, Reddy SS, Krishna BS, Naidu RM, Raju CN, Ghosh S. Synthesis of Schiff's bases in aqueous medium: a green alternative approach with effective mass yield and high reaction rates. Green Chem Lett Rev. 2010; 3(3): 217-223.

10. Shakir RM, Ariffin A, Ng SW. Ethyl 4-[(3, 5-di-tert-butyl-2-hydroxybenzyl)amino]benzoate. Acta Crystallogr, Sect E: Struct Rep Online. 2010; 66(11): o2916-o2916.

11. Shakir RM, Saoud SA, Hussain DF, Ali KF, Algburi FS, Jasim HS. Synthesis, Antioxidant ability and Docking study for new 4, 4'-((2-(Aryl)-1H-benzo [d] imidazole-1, 3 (2H)-diyl) bis (methylene)) diphenol. Res J Chem Environ. 2022; 26(10): 10.

12. Sarhan B, Waheed E, Naema B. Synthesis and characterization of some mixed-ligand complexes contining N-acetyl tryptophane and α-picoline with some metal salts. IHJPAS. 2011; 24(1): 144-154.

13. Qadir KSH, Marouf BH. Efficacy and Safety of Thymoquinone on Suppression of Tumor Growth in N-butyl-N-(4-hydroxybutyl)-Nitrosamine-Induced Bladder Cancer in Rats. IJPS. 2023; 32(2): 150-161.

14. Ahmad S, Khan M, Rehman NU, Ikram M, Rehman S, Ali M, et al. Design, Synthesis, Crystal Structure, In Vitro and In Silico Evaluation of New N′-Benzylidene-4-tert-butylbenzohydrazide Derivatives as Potent Urease Inhibitors. Molecules. 2022; 27(20): 6906.

15. Koksharova T, Slyvka Y, Savchenko O, Mandzii T, Smola S. 5-Sulfosalicylato Cu (II), Zn (II) and Ni (II) coordination compounds with benzohydrazide: Synthesis, structure and luminescent properties. J Mol Struct. 2023; 1271: 133980.

16. Saad AH, Salih H. Adherence and Beliefs to Adjuvant Hormonal Therapy in Patients with Breast Cancer: A Cross-Sectional Study (Conference Paper). IJPS. 2021; 30(Suppl.): 31-39.

17. Sarhan BM, Kadhim NJ, Wheed EJ. Stability constant of some Metal Ion Complexes of (6-(2Amino-2-(4-hydroxyphenyl)-acetamido)-3,3--dimethyl-7oxo-4-thia-1-aza-bicyclo[3,2,0] heptanes-2carboxylic acid (Amoxicillin). IHJPAS. 2017; 26(3): 245-253.

18. Abdallah M, Haffar D, Benghanem F, Ghedjati S. Synthesis, characterization, antioxidant activities and DFT calculations of 2, 4-bis (2-hydroxy-3-methoxy benzaldehyde) diiminotoluene Schiff base. J Iran Chem Soc. 2023; 20(4): 897-910.

19. Nguyen QT, Pham PN, Bui QD, Nguyen VT. Synthesis, Spectral Characterization, and Biological Activities of Some Metal Complexes Bearing an Unsymmetrical Salen-Type Ligand,(Z)-1-(((2-((E)-(2-Hydroxy-6-methoxybenzylidene) amino) phenyl) amino) methylene) Naphthalen-2 (1H)-one. Heteroat Chem. 2023; 23: 1-8.

20. Wu X, Xu F, Yang Z, Ke Z, Shi L, Ye C, et al. Synthesis, biological evaluation, and molecular docking of ((4-([1, 2, 4] triazolo [4, 3-b][1, 2, 4, 5] tetrazin-6-yl) piperazin-1-yl) methyl) benzohydrazide derivatives. J Chem Res. 2020; 44(9): 543-550.

21. Ahmed AA, Waheed EJ, Numan AT. Synthesis, Characterization, Antibacterial study and Efficiency of Inhibition of New di-β-enaminone Ligand and its Complexes. J Phys Conf Ser. 2020: IOP Publishing.

22. Hashim DJ, Waheed EJ, Hadi AG, Baqir SJ. Exploring the biological activity of organotin carboxylate complexes with 4-sulfosalicylic acid. Bull Chem Soc Ethiop. 2023; 37(6): 1435-1442.

23. Waheed E, Farhan M, Hameed G. Synthesis and characterization of new manganese (II), cobalt (II), cadmium (II) and mercury (II) complexes with ligand [N-(3-acetylphenylcarbamothioyl)-2-chloroacetamide] and their antibacterial studies. J Phys Conf Ser; 2019: IOP Publishing.

24. Ahmad MS, Siddique AB, Khalid M, Ali A, Shaheen MA, Tahir MN, et al. Synthesis, antioxidant activity, antimicrobial efficacy and molecular docking studies of 4-chloro-2-(1-(4-methoxyphenyl)-4, 5-diphenyl-1 H-imidazol-2-yl) phenol and its transition metal complexes. RSC Adv. 2023; 13(14): 9222-9230.

25. Nawras A, Enass, JW, Synthesis, Characterization, Thermal and Biological Study of New Organic Compound with Some Metal Complexes. Int J Drug Deliv Technol. 2021; 11(2): 401-408.

26. Frisch M, Trucks G, Schlegel H, Scuseria G, Robb M, Cheeseman J, et al. Gaussian 16, Revision A. 03, Gaussian, Inc, Wallingford CT. 2016; 3.

27. Al-Khazraji AMA. Synthesis of Co(ll), Ni(ll), Cu(ll), Pd(ll), and Pt(lV) Complexes with 1^4,1^5,3^4,3^5-Tetrahydro-1^1*H*,3^1*H*-4,8-diaza-1,3(3,4)-ditriazola-2,6(1,4)-dibenzenacyclooctaphane-4,7-dien-1^5,3^5 -dithione, and the Thermal Stability of Polyvinyl Chloride Modified Complexes. Indones J Chem. 2023; 23(3): 754-769.

28. Yusuf TL, Oladipo SD, Zamisa S, Kumalo HM, Lawal IA, Lawal MM, et al. Design of new Schiff-Base Copper (II) complexes: Synthesis,

crystal structures, DFT study, and binding potency toward cytochrome P450 3A4. ACS omega. 2021; 6(21): 13704-13718.

29. Soto-Acosta S, Campos-Gaxiola JJ, Reynoso-Soto EA, Cruz-Enríquez A, Baldenebro-López J, Höpfl H, et al. Synthesis, Crystal Structure, DFT Studies and Optical/Electrochemical Properties of Two Novel Heteroleptic Copper (I) Complexes and Application in DSSC. Crystals. 2022; 12(9): 1240.

30. Junaid A, Ng CH, Ooi IH. Synthesis and Characterization of the Nanogold-Bound Ternary Copper (II) Complex of Phenanthroline and Cysteine as Potential Anticancer Agents. ACS omega. 2022; 7(30): 26190-26200.

31. Ramdas K, Reddy R, Sireesha B. Synthesis, Characterization, DNA Binding, Cleavage, Antibacterial, In vitro Anticancer and Molecular Docking Studies of Ni (II), Cu (II) and Zn (II) Complexes of 3, 4, 5-Trimethoxy-N-(3-Hydroxy-5-(Hydroxymethyl)-2-Methylpyridin-4-yl)methylene) Benzohydrazide. Arab J Sci Eng. 2022: 1-12.

32. Omar SK, Enass JW. Synthesis, spectroscopic characterization, molecular docking, antioxidant and anticancer studies of some metal complexes from tetraazamacrocyclic Schiff base ligand. Oncology and Radiotherapy. 2023; 17(11): 001-013.

33. Sarhan BM, Lateef SM, Waheed EJ. Synthesis and characterization of Some Metal Complexes of [N-(1,5-dimethyl-3-oxo-2-phenyl-2,3-dihydro-^{1}H-pyrazol4-ylcarbamothioyl)acetamide]. IHJPAS. 2017; 28(2): 102-115.

34. Awf AR, Enass JW, Ahmed TN. Synthesis, Characterization and Anticorrosion Studies of New Co(II), Ni(II), Cu(II), and Zn(II) Schiff Base Complexes. Int J Drug Deliv Technol. 2021; 11(2): 414-422.

تحضير, تشخيص وفعالية مضادات السرطان لبعض المعقدات الفلزية لليكاند الجديد المشتق من ٤-ميثيل بنزوهيدرازيد مع الدراسات الحسابية

ايناس جاسم وحيد*[١،]

[١]قسم الكيمياء، كلية التربية للعلوم الصرفة – ابن الهيثم، جامعة بغداد، بغداد، العراق

الخلاصة

الهدف من البحث تحضير مجموعة من المعقدات ذات الصيغة العامة [M(HMB)n]حيث M=VO(II),Cr(III) and Cu(II) بينما n=2,3,2 على التوالي الناتجة من تفاعل ليكاند جديد [ن--٢)هيدروكسي-٣-ميثوكسي بنزيل)-٤-ميثيل بنزوهيدرازيد] (HMB) المشتق من تفاعل المادتين (٤-ميثيل بنزوهيدرازيد و٢-هيدروكسي-٣- ميثوكسي بنزالدهايد) مع الايونات الفلزية. تم تشخيص المركبات المحضرة بعدة طرق طيفية منها الرنين المغناطيسي النووي، الكتلة، الأشعة تحت الحمراء، والأطياف الإلكترونية. من نتائج القياسات اقترحت الاشكال الهندسية المختلفة للمعقدات المحضرة مثل المربع المستوي (النحاس)، الهرم (الفناديل) والثماني السطوح (الكروم). دعمت عمليات حسابات نظرية الكثافة الوظيفية الأدلة التجريبية. تم تحسين هندسة الليكاند(HMB) والمعقدات الفلزية بدقة باستخدام برنامج كاوس ٠٩ في حسابات نظرية الكثافة الوظيفية، كما تم تحديد العديد من الخصائص الجزيئية أيضًا. أظهرت النتائج أن المعقدات الفلزية التي تم فحصها أكثر استقرارا من الليكاند الحر (HMB). تم استخدام الالتحام الجزيئي على بروتينات بكتريا الإشريكية القولونية والمكورات العنقودية الذهبية لتقدير طاقة الارتباط المحتملة للمثبطات. تمت دراسة نشاط المركبات المحضرة في تثبيط أنواع مختلفة من البكتيريا السالبة الإشريكية القولونية والموجبة المكورات العنقودية الذهبية حيث أظهرت الدراسات أن معقد النحاس اقوى قدرة على تثبيط كلا النوعين من البكتيريا مقارنة بالليكاند (HMB). تم فحص الليكاند ومعقد النحاس لمعرفة النشاط المضاد للسرطان ضد خط خلايا سرطان الكبد البشري والخلايا الطبيعية.

الكلمات المفتاحية: : فعالية مضادات السرطان،نظرية الكثافة الوظيفية،المعقدات الفلزية، ٤-مثيل بنزوهايدرازيد، الالتحام الجزيئي.